


Three-dimensional universality class of the Ising model with power-law correlated critical disorderWenlong Wang ,* Hannes Meier, Jack Lidmar , and Mats Wallin *Department of Physics, Royal Institute of Technology, SE-106 91 Stockholm, Sweden* (Received 13 August 2019; revised manuscript received 14 October 2019; published 30 October 2019)

We use large-scale Monte Carlo simulations to test the Weinrib-Halperin criterion that predicts new universality classes in the presence of sufficiently slowly decaying power-law correlated quenched disorder. While new universality classes are reasonably well established, the predicted exponents are controversial. We propose a method of growing such correlated disorder using the three-dimensional Ising model as a benchmark system for both generating disorder and studying the resulting phase transition. Critical equilibrium configurations of a disorder-free system are used to define the two-value distributed random bonds with a small power-law exponent given by the pure Ising exponent. Finite-size scaling analysis shows a new universality class with a single phase transition, but the critical exponents $\nu_d = 1.13(5)$, $\eta_d = 0.48(3)$ differ significantly from theoretical predictions. We find that depending on the details of the disorder generation, disorder-averaged quantities can develop peaks at two temperatures for finite sizes. Finally, a layer model with the two values of bonds spatially separated in halves of the system genuinely has multiple phase transitions, and thermodynamic properties can be flexibly tuned by adjusting the model parameters.

DOI: [10.1103/PhysRevB.100.144204](https://doi.org/10.1103/PhysRevB.100.144204)**I. INTRODUCTION**

Disordered systems have fascinating properties that can differ significantly from those of pure systems and can produce novel experimentally relevant effects. For example, disorder frequently generates new universality classes and can even completely alter the nature of phase transitions. Most studies of disordered systems concern independent random disorder, but if disorder correlations are present, the issue arises of when and how these are relevant. This paper focuses on spatial power-law correlated quenched disorder that can arise, e.g., from linear or planar dislocations in a crystal or for fluids in porous media. Such disorder is characterized by an exponent a ; that is, the correlation function of the defects decays as $g(r) \sim 1/r^a$.

A few guiding theories are available. The Harris criterion [1] states that weak uncorrelated disorder is irrelevant if the heat capacity exponent of the corresponding pure, disorder-free system is negative, $\alpha_{\text{pure}} < 0$, or the correlation length exponent $\nu_{\text{pure}} > 2/d$ assuming the hyperscaling relation $d\nu = 2 - \alpha$. For power-law correlated disorder, this is generalized to the Weinrib-Halperin (WH) criterion [2], which predicts that weak disorder is irrelevant if the pure system satisfies $\nu_{\text{pure}} > \max(2/a, 2/d)$. Moreover, when disorder is relevant, a new disordered universality class is obtained if $a < d$ with exponents given by $\nu_d = 2/a$ and $\eta_d = 0$. A number of papers have tested this criterion by numerical simulations. While it seems reasonably well established that a new universality class is indeed obtained for the three-dimensional Ising model with oriented line disorder corresponding to $a = 2$ [3–5], it is quite controversial whether $\nu_d = 2/a$ holds. For example, it has been argued that the result is merely a first-order estima-

tion, ignoring higher-order corrections [6–8]. See Ref. [5] and the references therein for a more detailed discussion.

In this work we study power-law correlated quenched disorder generated from equilibrium spin configurations of a pure, i.e., disorder-free, zero-field Ising model at the phase transition. This correlated disorder distribution avoids possible ambiguities due to, e.g., linear correlated defects crossing and is much more straightforward to generate in simulations. In addition, the decay exponent is $a \approx 1$ (see below), which is much smaller than that of line defects. Therefore, the predicted exponent $\nu_d \approx 2$ is extraordinarily large, which is ideal for testing the WH criterion. A similar idea of using an auxiliary model to grow power-law correlated disorder was used in previous studies of correlated random models. A three-dimensional (3D) Ising model with correlated random dilution was studied in Ref. [9]. Potts models in two dimensions were studied in Refs. [10,11]. Here, we study the different case of a random bond Ising model in three dimensions.

To define the disorder distribution, equilibrium spin configurations of a pure Ising model at the critical point are mapped onto quenched random couplings of a disordered Ising system that, by construction, become power-law correlated. We discuss the generating method in detail in the following sections. The random couplings are defined to take two values corresponding to the two spin orientations in the underlying Ising configuration. While this disorder model does not fulfill the WH assumption of a Gaussian disorder distribution, the WH results are still useful guides, and it is of interest to compare results. For simplicity we restrict our study to ferromagnetic couplings in this paper; that is, there is no frustration, and the ground state is the same ferromagnetic state as for the pure system. The power-law decay of the random couplings to leading order follows from the pure spin correlation function exponent $a = d - 2 + \eta_{\text{pure}}$. For the pure Ising model in three dimensions $a = 1.036298(2)$, and

*wenlongcmp@gmail.com

$a < d$ is satisfied. The WH criterion therefore predicts for the disordered system a single phase transition with a new exponent, $\nu_d \approx 1.9299$. The critical cluster distribution leads to formation of power-law correlated domains of strong and weak bonds in the random Ising model. Here, this model is studied theoretically to demonstrate what effects are, in principle, possible, without considering how it may be realized in practice.

The main purpose of this paper is to investigate the universality class of the phase transition in the three-dimensional Ising model with correlated bond disorder generated from pure Ising configurations and in particular to identify the role of disorder correlations by comparing several different but related models. We use Monte Carlo simulations and finite-size scaling to study critical properties at the transition. For correlated disorder a new universality class of the Ising phase transition emerges, as expected from the WH theory, but the values of the exponents do not follow the WH results. Notably, the finite-scaling approach to the thermodynamic limit is unusual in the following sense. Quantities such as the susceptibility and heat capacity usually have a single rounded and finite peak close to the transition temperature for finite system sizes. Here, instead, such disorder-averaged quantities can obtain peaks at two different temperatures for finite systems. The two peak temperatures are system size dependent and merge in the thermodynamic limit, so the infinite system has a single phase transition, as expected from the WH theory. In addition to the correlated disorder model, we also study a layer model with the two values of bonds spatially separated to layers. The layer model is not disordered and trivially has two thermodynamic transitions and double peaks in the susceptibility that are not finite-size effects. By selecting the values of the couplings and the number of layers, great flexibility to engineer the thermodynamic properties of the system is demonstrated. In particular several susceptibility peaks can be produced, which is potentially relevant for magnetic applications.

An additional purpose is to investigate the performance of two different Monte Carlo algorithms, the parallel tempering (PT) method [12–14] and the recently introduced population annealing (PA) method [15–19]. These methods have been used extensively to simulate spin-glass problems and similar problems with frustration and complex ground states where it has been found that PA and PT have similar efficiency [18,20]. Here, we consider the case of correlated disorder with no frustration that preserves the ferromagnetic ground state and compare the performance of both methods.

This paper is organized as follows. We first discuss the models, observables, and simulation methods in Sec. II, followed by numerical results in Sec. III. Concluding remarks are stated in Sec. IV.

II. MODELS, OBSERVABLES, AND METHODS

A. Models

The Ising Hamiltonian is

$$H = - \sum_{\langle ij \rangle} J_{ij} S_i S_j, \quad (1)$$

where $S_i = \pm 1$ are Ising spins and the summation is over nearest neighbors on a three-dimensional cubic lattice with side length L and $N = L^3$ sites. For the pure system with $J_{ij} = 1$ the critical temperature and critical exponents are known to high precision. We take $\beta_{c,\text{pure}} = 0.22165455(3)$ obtained from Monte Carlo simulations [21] to generate critical configurations of the pure system. It is noted that this critical inverse temperature slightly deviates from the most recent estimates [22,23], but it is sufficiently accurate for our purpose. The conformal bootstrap method provides high-precision estimates of critical exponents for the Ising model given by $\nu_{\text{pure}} = 0.629971(4)$ and $\eta_{\text{pure}} = 0.036298(2)$ [24]. We refer to these quantities for the disordered system as β_c , ν_d , and η_d , respectively.

The correlated quenched random couplings J_{ij} are defined as follows:

(1) Simulate the pure 3D Ising model and generate equilibrium configurations at the phase transition.

(2) Define a set of random coupling constants from an equilibrium spin configuration of the pure model. For bonds within spin-up clusters set $J_{ij} = 2$, and otherwise, $J_{ij} = 1$, i.e., within spin-down clusters and at cluster boundaries. More precisely, $J_{ij} = 1 + (S_i + 1)(S_j + 1)/4$.

The resulting values $J_1 = 1$, $J_2 = 2$ are fixed unless otherwise specified. We refer to J_1 as weak bonds and J_2 as strong bonds. This method to define random couplings from underlying pure Ising configurations is not unique. The method leads to an asymmetry in the fraction of J_1 and J_2 bonds due to the treatment of the interfaces. It is possible to eliminate this asymmetry. One simple way is to let a single spin determine the bonds in the forward directions of each axis. For example, set a forward bond to J_2 if a spin takes the value 1 and J_1 if it is -1 . We call the asymmetric version pair disorder and the forward version forward disorder. We simulated these and some other disorder models with variations of the short-range details and found they have similar properties. Note in particular that the forward disorder inherits directly the bond correlation function $G_{ik} = \langle s_i s_k \rangle - \langle s_i \rangle \langle s_k \rangle \sim |\mathbf{r}_i - \mathbf{r}_k|^{2-d-\eta_{\text{pure}}}$ from spins of the pure model to bonds of the disordered model. For the pair disordered model the bond correlation function is $\langle J_{ij} J_{kl} \rangle - \langle J_{ij} \rangle \langle J_{kl} \rangle = (G_{ik} + G_{il} + G_{jk} + G_{jl} + G_{ij,kl}^E)/16$, where $G_{ij,kl}^E = \langle (s_i s_j - \langle s_i s_j \rangle)(s_k s_l - \langle s_k s_l \rangle) \rangle$ is proportional to the correlation function for the energy density of the pure Ising model, which scales as $r^{-2(d-1/\nu_{\text{pure}})} \approx r^{-2.83}$. The contribution from G^E will thus quickly decay compared to the leading power-law behavior r^{-a} . The data shown here are for pair disorder unless otherwise specified.

We considered a few variations in the definition of the bond disorder distribution corresponding to different spin ensembles of the underlying pure Ising model. Here, we illustrate this using the forward disorder. If the disorder-generating Ising configurations have no restriction in the net magnetization, the different disorder realizations will obtain varying numbers of strong and weak bonds, which we call the unrestricted or $M \neq 0$ disorder. If the generating spins are restricted to zero magnetization, each disorder realization has equal numbers of strong and weak bonds. We call this restricted or $M = 0$ disorder.

For comparison with the random distribution of the couplings, we also considered a layer model which is not disordered by distributing couplings in a nonrandom way. Here, all couplings are assigned to J_1 in the upper half of the system and J_2 in the lower half. This is essentially two pure Ising models connected by flat interfaces between regions with weak and strong bonds. The layer model can be generalized in different ways, e.g., by changing sizes of layers, adding more layers, and using more values of the couplings. If the number of spins in each layer is proportional to the total volume L^3 , the ratio of the number of interface to bulk couplings disappears as $1/L$, and each layer trivially obtains its own thermodynamic bulk Ising transition at a critical temperature related to the coupling constant in the layer. Thus, the n -layer model can have a sequence of n transitions where the net magnetization changes in a staircase manner as temperature is varied.

B. Observables and methods

The main observables are the absolute value of the magnetization density m , Binder ratio g , magnetic susceptibility χ , and heat capacity c . These quantities are defined as

$$m = \frac{1}{N} \left| \sum_i S_i \right|, \quad (2)$$

$$g = \frac{\langle m^4 \rangle}{\langle m^2 \rangle^2}, \quad (3)$$

$$\chi = \beta N [\langle m^2 \rangle - \langle |m| \rangle^2], \quad (4)$$

$$c = \frac{\beta^2}{N} [\langle H^2 \rangle - \langle H \rangle^2]. \quad (5)$$

Averages are performed over thermal fluctuations denoted $\langle \dots \rangle$ and over quenched disorder denoted $[\dots]$.

The finite-size scaling relations for computing critical exponents are summarized as follows:

$$g(t) = g(tL^{1/\nu}), \quad (6)$$

$$\chi(t) = L^{2-\eta} \chi(tL^{1/\nu}), \quad (7)$$

$$g_T(t=0) = \left. \frac{\partial g}{\partial T} \right|_{t=0} \sim L^{1/\nu}, \quad (8)$$

$$\chi(t=0) \sim L^{2-\eta}, \quad (9)$$

where $t = (T - T_c)/T_c$ is the reduced temperature and T_c is the phase transition temperature. We measure g_T using its direct estimator $\partial \langle O \rangle / \partial T = \beta^2 [\langle OH \rangle - \langle O \rangle \langle H \rangle]$, where O is any temperature-independent quantity, here m^2 or m^4 .

Our simulations are carried out using two different Monte Carlo (MC) methods, population annealing [15–19] and parallel tempering [12–14] with hybrid Metropolis and Wolff updates. The two methods give consistent results, and both are in agreement with the known results of the pure system for the transition temperature and the critical exponents. Since PT is widely used and well known, here, we discuss only the relatively new PA method.

The PA method works as follows. We initialize R random configurations or replicas at $\beta = 0$. The population of

replicas is cooled gradually following an annealing schedule. When the temperature is decreased from β to β' , a replica is copied with the expectation number $n_i = \exp[-(\beta' - \beta)E_i]/Q$, where E_i is the energy of replica i and $Q = (1/R) \sum_i \exp[-(\beta' - \beta)E_i]$ is a normalization factor to keep the population size approximately the same throughout the annealing. In our simulation, the number of copies is either the floor or the ceiling of n_i to minimize fluctuations with the proper probabilities to give the correct mean value. After this resampling step, N_S sweeps using the Metropolis algorithm are applied to each replica. In the temperature range where the Wolff update [25] is efficient, we also apply N_S Wolff updates to each replica. The two hybrid updates alternate with one Metropolis sweep and one Wolff update. The annealing process continues with resampling and Monte Carlo sweeps until reaching the lowest temperature.

Our equilibration criterion for PA is based on the family entropy, which quantifies the diversity of the population. In the initial population, each replica is assigned a family name $1, 2, 3, \dots, R$. The family name is copied along with the replica in the annealing process. At each stage of the simulation, we can collect the fraction of each family name in the population $\{f_i\}$, and the family entropy S_f is then the regular Gibbs entropy $S_f = -\sum_i f_i \ln(f_i)$ [18,26]. The larger S_f is, the better the equilibration is. We require each annealing to satisfy $S_f \geq \ln(100)$. To prevent correlations when generating the disordered instances, we have recorded only 500 configurations from the much larger population for each simulation of the pure system, and more configurations are collected using independent runs. For PT we used at least 10^5 sweeps for thermalization before data collection. We record one equilibrium configuration for every 10^4 sweeps at each temperature and also save 500 configurations for each independent run. The simulation parameters are summarized in Table I. Note that PA is massively parallel as different replicas can be updated independently. The PA is implemented with distributed-memory MPI parallel computing [27], and PT is implemented with shared-memory OPENMP parallel computing [28].

III. NUMERICAL RESULTS

In this section, we first demonstrate that there is a single phase transition in three dimensions. Next, we study the critical behavior of the transition and compare it with the WH criterion. Finally, we discuss the layer model and compare the efficiency of the PA and PT methods.

A. Correlated disorder

We first show some typical and disorder-averaged MC results for the magnetization, heat capacity, and susceptibility for the correlated disorder model for system size $L = 14$ in Fig. 1. The disorder averages are marked with red dots and form thick red curves. The thin curves are data for five individual disorder samples. The most noticeable feature of the disorder-averaged curves is the two-peak structure present for both the heat capacity and susceptibility, indicating two characteristic temperatures. However, each individual sample has only one peak or transition. The emergence of this

TABLE I. Simulation parameters of the three-dimensional Ising model using population annealing (PA) and parallel tempering (PT) for the pure and disordered systems with pair disorder. L is the linear system size, R is the number of replicas, N_T is the number of temperatures, and N_S is the number of sweeps. The temperature range is $\beta \in [\beta_{\min}, \beta_{\max}]$, and the Wolff updates are applied in the interval $\beta \in [\beta_1, \beta_2]$. Finally, M is the number of independent runs or disorder realizations studied.

System	Algorithm	L	R	N_T	N_S	β_{\min}	β_{\max}	β_1	β_2	M
Pure	PA	{4, 6, 8}	8×10^5	101	10	0	0.4	0.2	0.3	20
Pure	PA	{10, 12, 14, 16, 18}	1.6×10^6	201	10	0	0.4	0.2	0.3	20
Pure	PA	{20, 24}	1.6×10^6	301	10	0	0.4	0.2	0.3	20
Pure	PA	{28, 32}	1.6×10^6	301	10	0	0.25	0.2	0.25	20
Pure	PT	{36, 40, 44, 50}	16		6×10^6	0.2	0.24	0.2	0.24	20
Disorder	PA	{4, 6, 8}	8×10^5	101	10	0	0.4	0.1	0.3	5000
Disorder	PA	{10}	1.2×10^6	201	10	0	0.4	0.1	0.3	3000
Disorder	PA	{12, 14, 16}	1.2×10^6	201	10	0	0.3	0.1	0.2	3000
Disorder	PA	{18, 20}	1.2×10^6	201	10	0	0.22	0.1	0.2	2000
Disorder	PT	{24, 28, 32}	32		1.1×10^6	0.13	0.15	0.13	0.15	2000
Disorder	PT	{36, 40, 44, 50}	32		2.2×10^6	0.13	0.15	0.13	0.15	2000

double-peak structure is one main result of this paper and will now be analyzed in more detail.

Interestingly, the two peak structures after careful inspections are finite-size effects, and there is a single phase transition in the thermodynamic limit $L \rightarrow \infty$. This is first indicated by the fact that each individual disorder realization has only one peak. The peak temperature reflects the average strength of the bonds of the disorder realization. Moreover, the two peak temperatures of the disorder averages move closer together as the system size increases; see Fig. 2 for more details. The peak at low (high) β is associated with disorder realizations with a majority of strong (weak) bonds.

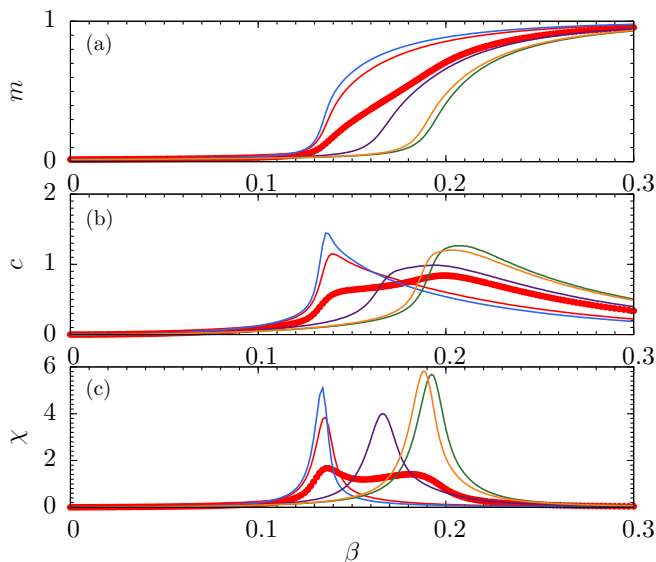


FIG. 1. Typical and disorder-averaged results for (a) the absolute value of the magnetization, (b) heat capacity, and (c) susceptibility of the correlated disorder model for system size $L = 14$. The red dots are the disorder-averaged data, and the thin curves are for five individual disorder realizations. The average magnetization has a finite-size rounded two-step temperature dependence. The disorder averages in (b) and (c) have peaks at the two magnetization steps, while individual disorder realizations have one peak.

To further demonstrate the two peaks are finite-size effects, we also studied a restricted disorder model which always has equally many strong and weak bonds from the disorder-generating pure-spin model. In Ref. [29] such constraints were

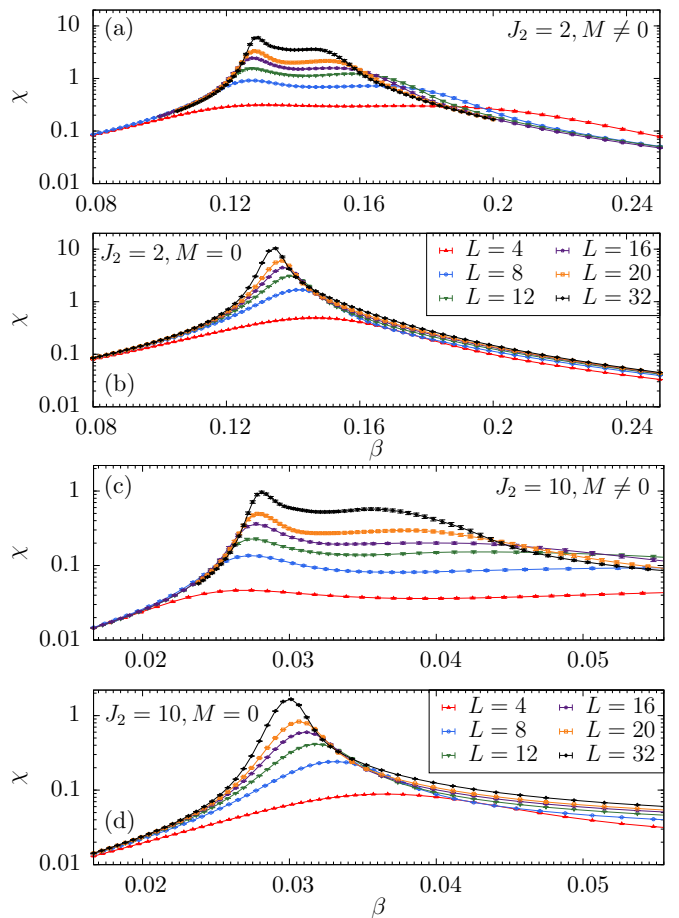


FIG. 2. Disorder-averaged susceptibility for comparing cluster disorder ($M \neq 0$) and restricted cluster disorder ($M = 0$). Here, we examine two strong bond strengths and use the forward disorder. The two ensembles of disorder have the same thermodynamic limit, and there is therefore only one phase transition.

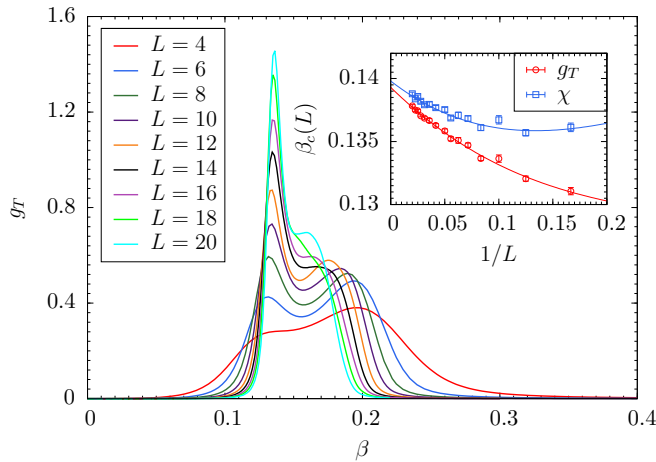


FIG. 3. Disorder-averaged g_T vs β has a two-peak structure for small system sizes. The left peak dominates for the large system size and is used to estimate the size-dependent transition temperature. A similar estimate is done for χ . Inset: The extracted pseudotransition temperature (symbols) of the left peak vs $1/L$ along with a cubic fit (curves), giving $\beta_c = 0.1393(3)$ and $0.1398(4)$ from the fits of g_T and χ , respectively. The $L = 4$ data are omitted from the fit as there is no clear left peak for this size.

found not to affect the universality class of the transition in the similar problem of a diluted 3D Ising model with long-range disorder. Results for the disorder-averaged susceptibility of the restricted disorder model are shown in Fig. 2 for the forward models with both $J_2 = 2$ and $J_2 = 10$. Clearly, only one peak is obtained for any system size, and the same is true for the individual disorders. It is remarkable that this is the case even for the extraordinarily large strong bonds $J_2 = 10$. From Fig. 2 it is also plausible that the transition temperatures of the two different disorder-generating ensembles converge to the same values for $L \rightarrow \infty$. Here, the unrestricted ensemble has the two peaks originating from the two-peak distribution of the magnetization of the underlying pure model, and in the restricted ensemble this is eliminated. This concludes the demonstration that the two peaks found above are finite-size effects caused by the disorder-averaging procedure and the disorder-generation method, and in the thermodynamic limit there is a single transition.

B. Critical exponents

The next step is to study the finite-size scaling of the phase transition. The main objective is to estimate the critical exponents at the transition by finite-size scaling of the susceptibility and Binder parameter derivative. We consider finite-size scaling at the thermodynamic critical temperature. According to Eqs. (8) and (9), the scaling at the critical temperature is $\chi \sim L^{2-\eta}$, and $g_T \sim L^{1/\nu}$. We have used the unrestricted pair disorder for this major large-scale simulation.

The first step is to estimate the thermodynamic transition temperature. We use the major high-temperature peaks of g_T and χ to estimate β_c . Data for g_T vs $\beta = 1/T$ for a series of sizes are shown in the main panel of Fig. 3. Similar behavior is found for χ (data not shown). It is seen that two peaks obtained for small sizes successively merge upon increasing

the system size, and the left peak at low β dominates for large system sizes. Hence, the temperature of the left peak should extrapolate to the thermodynamic transition temperature for $L \rightarrow \infty$. Using cubic spline interpolation, a pseudotransition inverse temperature $\beta_c(L)$ is computed by locating the maximum for each quantity and system size. Error bars are estimated using the bootstrap method. Ideally, one would like to estimate the thermodynamic transition temperature using the scaling relation $\beta_c(L) = \beta_c + a/L^{1/\nu_d}$, but this requires simultaneous fits of β_c and ν_d , which leads to large statistical errors for this disordered model. We instead adopt a cubic polynomial fit in $1/L$ and extrapolate to $1/L = 0$ (see the inset in Fig. 3). The validity of this method was verified using the scaling fits assuming $\nu_d = 1.13$ estimated below, with consistent results within error bars. We also verified that this method reproduces known results reliably for both the critical temperature and critical exponents of the corresponding pure model. The results for the correlated disordered model are $\beta_c = 0.1393(3)$ and $0.1398(4)$ from the fits of g_T and χ , respectively. The results agree within error bars, and we combine the two and estimate $\beta_c = 0.1396(3)$, which is close to the simple estimate $(2/3)\beta_{c,\text{pure}} = 0.1478$ given by the mean bond value.

Our main results for critical exponents are summarized in Fig. 4. Notice that to a good approximation a power law is obtained for g_T , while substantial deviations from a pure power law are found in the data curve for χ for small system sizes, indicating the presence of scaling corrections. Including data points for the seven largest system sizes where a power-law fit is reasonably justified gives

$$\nu_d = 1.13(5), \quad \eta_d = 0.48(3). \quad (10)$$

Error bars are bootstrap estimates of the statistical errors. Note that the exponents differ significantly from both the pure universality class and the WH results. In particular, the exponent ν_d sits in between these two values. This behavior is similar to recent results for models with line defects [4,5].

For uncorrelated disorder recent simulation estimates [30] of the exponents for the 3D Ising model with bond disorder are $\nu = 0.685(7)$ and $\gamma/\nu = 1.964(9)$, which gives $\eta = 2 - \gamma/\nu = 0.036(9)$. These values are significantly different from the values obtained here for correlated disorder, showing that the long-range correlations are relevant and change the universality class as expected.

Next, we consider data collapses to verify that the estimated exponents hold. It is useful to plot g_T and χ vs g in order to eliminate explicit temperature scaling. The results are shown in Fig. 4. A scaling collapse onto a common function for each quantity is found around the phase transition. This confirms that the data fulfill the finite-size scaling assumption.

Summarizing, the correlated disorder model produces a new universality class that differs from the pure model. This agrees with the expectation from WH theory, but the critical exponents differ significantly from the WH prediction.

C. Bilayer model

In the previous section, the 3D Ising model with critical correlated disorder has two peaks in the disorder-averaged susceptibility for finite system size that merge into one

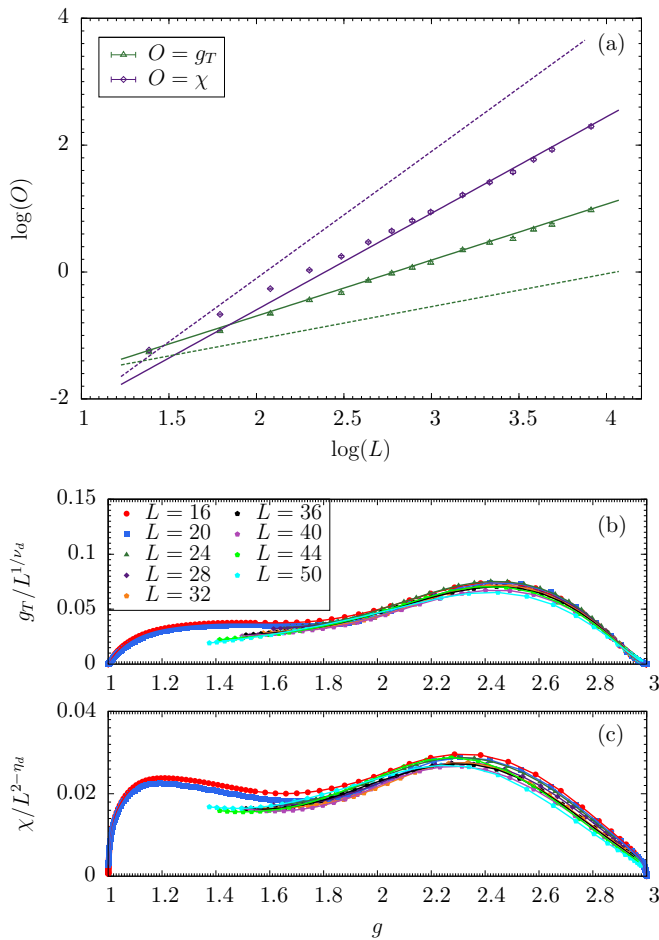


FIG. 4. (a) Scaling of g_T and χ with system size L at the thermodynamic transition temperature. The linear solid fits are done using the seven largest sizes, and the dashed lines are guiding lines with the predicted WH slopes. (b) and (c) Finite-size scaling data collapse of scaled quantities vs Binder ratio g . The sizes included are $L = 16, 20, 24, 28, 32, 36, 40, 44, 50$.

transition in the thermodynamic limit, while individual disorder realizations have a single peak. This motivates the problem of constructing a simpler disorder-free model with similar double-peak properties. This calculation also demonstrates that double-peak structure can occur also without bond imbalance. Here, the coupling constants are given different values in the equally large upper and lower half-spaces. In the top layer the bonds of each spin in the forward direction are fixed to $J_{\text{up}} = 1$, and in the bottom layer the bonds similarly are all set to, e.g., $J_{\text{dn}} = 2$. In contrast to the random model studied in the previous section there is no disorder. Periodic boundary conditions are used in all directions, so there are two boundaries between strongly and weakly coupled spins.

We studied a series of system sizes for $J_{\text{dn}} = 2$, and MC data for the heat capacity and susceptibility are shown in Fig. 5 for four representative sizes. There are clearly two peaks emerging, one at $\beta_{c,\text{pure}}$ and the other at $\beta_{c,\text{pure}}/2$. The layers are coupled only at the interfaces so that each layer trivially has an independent phase transition in the thermodynamic limit. Thus, the two-peak structure in the correlated disorder model can be reproduced in the simple layer model, but in

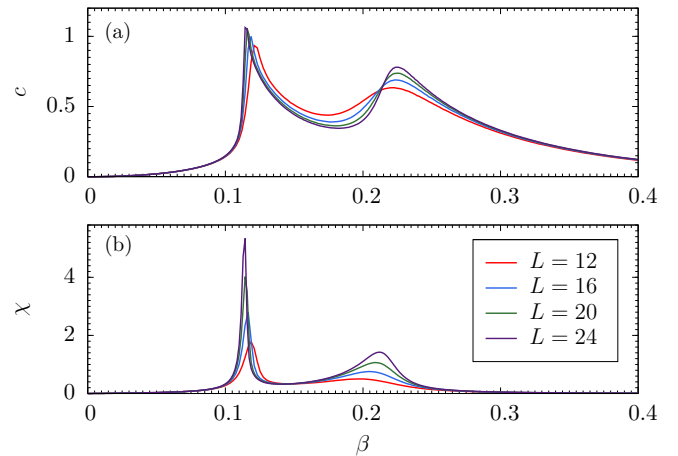


FIG. 5. Monte Carlo data for the bilayer Ising model with $J_{\text{up}} = 1$ and $J_{\text{dn}} = 2$. (a) Heat capacity. (b) Susceptibility. In contrast to the cluster disorder model the two peaks of the layer model indicate two phase transitions. Error bars are small and omitted for clarity.

contrast to the disordered case, the peaks of the layer model do not merge in the thermodynamic limit.

A useful feature of the layer model is that with two phase transitions the shape of the magnetization curve can be designed by selecting the coupling strengths. This is illustrated in Fig. 6, where the magnetization curve is shifted by tuning $J_{\text{dn}} = 1, 2, 3, 4$ while keeping $J_{\text{up}} = 1$ fixed. Since the system has two independent phase transitions, the magnetization in the thermodynamic limit is given by

$$m(\beta) = 1/2[m_0(\beta) + m_0(\beta J_{\text{dn}}/J_{\text{up}})], \quad (11)$$

where m_0 is the magnetization of the pure system.

It is straightforward to generalize to multiple layers, different layer volumes, etc. This permits engineering the magnetization curve to a desired shape. For p layers of strength J_i and weights ω_i , which is the fraction of the number of spins of layer i , the magnetization in the thermodynamic limit is

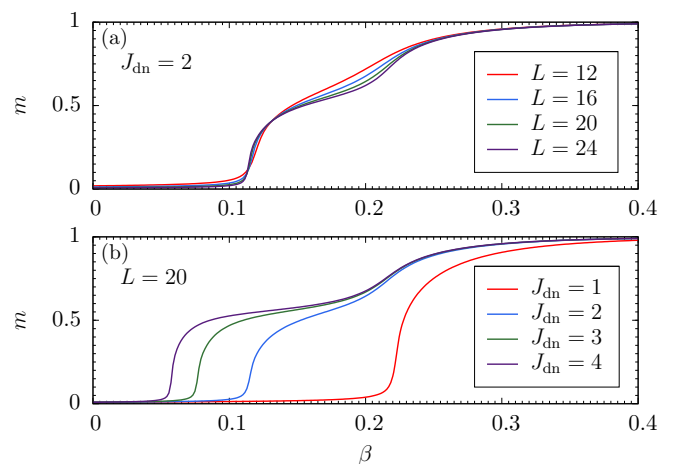


FIG. 6. (a) Magnetization curve for different sizes for $J_{\text{up}} = 1$ and $J_{\text{dn}} = 2$. (b) Dependence of the magnetization curve on J_{dn} for fixed $J_{\text{up}} = 1$ and system size $L = 20$. Error bars are small and omitted for clarity.

generalized to

$$m(\beta) = \sum_{i=1}^p \omega_i m_0(J_i \beta). \quad (12)$$

D. Efficiency of PA and PT

Our work has also changed our view regarding the efficiency of the PA and PT algorithms. The PA algorithm has been used successfully in a number of studies of spin glasses, a system that is both disordered and frustrated. It has been found that the two algorithms are quite similar in efficiency in both equilibrium samplings [18] and optimizations [20]. Here and in our recent work on two-dimensional monodisperse particles [31], where frustration is either fully absent or much weaker, we find that PT has an advantage over PA for studying phase transitions.

The key difference is the much shorter equilibration and autocorrelation times for less disordered and frustrated systems, where one can quickly equilibrate and start data collection using PT near the phase transitions. On the other hand, PA has to do the “temperature journey” and a large portion of work is “wasted” in this process. For example, to simulate a pure model only at the critical temperature it is clearly less efficient to use PA. On the other hand, for collecting data over a wide range of temperatures the two algorithms are again similar in efficiency. Therefore, PT can have an advantage over PA for studying phase transitions of pure or weakly disordered and frustrated systems, but the efficiency is similar for studying a wide range of temperatures or complex energy landscapes. In addition, PA has certain interesting features not shared by PT such as being massively parallel.

IV. CONCLUSIONS

In common model magnets the order parameter signals a transition from a magnetically ordered to disordered state as temperature is increased, and thermodynamic quantities such as the magnetization curve have little structure except for the singularity at the transition. For finite-size samples, for example, nanosize magnetic particles relevant in applications, divergent quantities become rounded with a single peak at the transition. Introduction of uncorrelated quenched random disorder may alter the universality class of the phase transition, but the qualitative features remain similar to the pure case. In this paper we pointed out that the presence of spatially correlated quenched disorder can alter this picture.

We considered power-law correlated critical cluster disorder generated from the equilibrium states at a second-order phase transition. We applied correlated critical cluster disorder as random bond couplings of a 3D Ising model. We found unusual double-peaked disorder-averaged susceptibility and other fluctuation quantities for finite system sizes but one phase transition in the thermodynamic limit. The appearance of the double peaks depends on the method of generating disorder but not on the disorder correlations. In particular, if

the disorder-generating configurations are restricted to zero magnetization, then disorder averages become single peaked.

From finite-size scaling of MC data we obtained $\nu_d = 1.13(5)$, $\eta_d = 0.48(3)$. For power-law correlated disorder with sufficiently slow decay as in our correlated disorder model, WH theory predicts a new long-range fixed point. This prediction agrees with our simulation results, but the predicted exponents disagree with our exponents, suggesting that the WH results need higher-order corrections to apply to our bimodal disorder distribution.

We also studied a bilayer model which has two susceptibility peaks, similar to the correlated disorder results. However, contrary to the critical disorder model the double-peak structure appears at a single sample level and persists in the thermodynamic limit, and there are therefore two separate phase transitions. Notably, the shape of the magnetization vs temperature curve can be modified by changing the parameters of the system. By straightforward generalization to multiple layers, we proposed a way to engineer the magnetization curve almost at will by tuning the coupling strength and weights of different layers. In addition, our two models showed that double peaks can be created from two different mechanisms: bond imbalance and bond correlation. Further investigations suggested that the two mechanisms are independent: (1) disordered models with no correlation but bond imbalance also show double peaks, and (2) correlated disorders, e.g., the layer model without bond imbalance, again show double peaks.

For two-dimensional Potts models with a disorder construction similar to that used here, Chatelain [10,11] obtained interesting hyperscaling violations related to the lack of self-averaging, and Griffiths phases. While we consider a different model, it is notable that we did not observe these effects in our 3D results. Using the scaling relation $m(t=0) \sim L^{-\beta_d/\nu_d}$, we estimate $\beta_d/\nu_d = 0.73(4)$, again using the seven largest sizes. The pertinent magnetic hyperscaling ($\gamma_d/\nu_d = d - 2\beta_d/\nu_d$) is well satisfied after applying $\gamma_d/\nu_d = 2 - \eta_d$.

The critical cluster disorder model can be readily applied in other dimensions and to other $O(N)$ models, e.g., by adding the Ising correlated disorder to the XY and Heisenberg models. It is also interesting to study spin glasses with such correlated disorder. Research along these lines is currently in progress and will be reported in future publications.

ACKNOWLEDGMENTS

W.W. acknowledges support from Swedish Research Council Grant No. 642-2013-7837 and the Goran Gustafsson Foundation for Research in Natural Sciences and Medicine. M.W. acknowledges support from Swedish Research Council Grant No. 621-2012-3984. The computations were performed on resources provided by the Swedish National Infrastructure for Computing (SNIC) at the National Supercomputer Centre (NSC), the High Performance Computing Center North (HPC2N), and the PDC Center for High Performance Computing.

[1] A. B. Harris, Effect of random defects on the critical behavior of Ising models, *J. Phys. C* **7**, 1671 (1974).

[2] A. Weinrib and B. I. Halperin, Critical phenomena in systems with long-range-correlated quenched disorder, *Phys. Rev. B* **27**, 413 (1983).

- [3] H. G. Ballesteros and G. Parisi, Site-diluted three-dimensional Ising model with long-range correlated disorder, *Phys. Rev. B* **60**, 12912 (1999).
- [4] V. V. Prudnikov, P. V. Prudnikov, B. Zheng, S. V. Dorofeev, and V. Y. Kolesnikov, Short-time critical dynamics of the three-dimensional systems with long-range correlated disorder, *Prog. Theor. Phys.* **117**, 973 (2007).
- [5] D. Ivaneyko, B. Berche, Yu. Holovatch, and J. Ilnytskyi, On the universality class of the 3d Ising model with long-range-correlated disorder, *Phys. A (Amsterdam, Neth.)* **387**, 4497 (2008).
- [6] V. V. Prudnikov and A. A. Fedorenko, Critical behavior of 3D systems with long-range correlated quenched defects, *J. Phys. A* **32**, L399 (1999).
- [7] V. V. Prudnikov, P. V. Prudnikov, and A. A. Fedorenko, Static and dynamic critical properties of 3D systems with long-range correlated quenched defects, *J. Phys. A* **32**, 8587 (1999).
- [8] V. V. Prudnikov, P. V. Prudnikov, and A. A. Fedorenko, Field-theory approach to critical behavior of systems with long-range correlated defects, *Phys. Rev. B* **62**, 8777 (2000).
- [9] M. I. Marqués, J. A. Gonzalo, and J. Íñiguez, Universality class of thermally diluted Ising systems at criticality, *Phys. Rev. E* **62**, 191 (2000).
- [10] C. Chatelain, Hyperscaling violation in the 2D 8-state Potts model with long-range correlated disorder, *Europhys. Lett.* **102**, 66007 (2013).
- [11] C. Chatelain, Griffiths phase and critical behavior of the two-dimensional Potts models with long-range correlated disorder, *Phys. Rev. E* **89**, 032105 (2014).
- [12] R. H. Swendsen and J.-S. Wang, Replica Monte Carlo Simulations of Spin Glasses, *Phys. Rev. Lett.* **57**, 2607 (1986).
- [13] C. Geyer, Markov chain Monte Carlo maximum likelihood, in *Computing Science and Statistics: 23rd Symposium on the Interface*, edited by E. M. Keramidas (Interface Foundation, Fairfax Station, VA, 1991), p. 156.
- [14] K. Hukushima and K. Nemoto, Exchange Monte Carlo method and application to spin glass simulations, *J. Phys. Soc. Jpn.* **65**, 1604 (1996).
- [15] K. Hukushima and Y. Iba, Population annealing and its application to a spin glass, in *The Monte Carlo Method in the Physical Sciences: Celebrating the 50th Anniversary of the Metropolis Algorithm*, edited by J. E. Gubernatis, AIP Conf. Proc. No. 690 (AIP, New York, 2003), p. 200.
- [16] E. Zhou and X. Chen, A new population-based simulated annealing algorithm, in *Proceedings of the 2010 Winter Simulation Conference (WSC)* (Springer, Baltimore, 2010), p. 1211.
- [17] J. Machta, Population annealing with weighted averages: A Monte Carlo method for rough free-energy landscapes, *Phys. Rev. E* **82**, 026704 (2010).
- [18] W. Wang, J. Machta, and H. G. Katzgraber, Population annealing: Theory and application in spin glasses, *Phys. Rev. E* **92**, 063307 (2015).
- [19] L. Y. Barash, M. Weigel, M. Borovský, W. Janke, and L. N. Shchur, GPU accelerated population annealing algorithm, *Comput. Phys. Commun.* **220**, 341 (2017).
- [20] W. Wang, J. Machta, and H. G. Katzgraber, Comparing Monte Carlo methods for finding ground states of Ising spin glasses: Population annealing, simulated annealing, and parallel tempering, *Phys. Rev. E* **92**, 013303 (2015).
- [21] Y. Deng and H. W. J. Blöte, Simultaneous analysis of several models in the three-dimensional Ising universality class, *Phys. Rev. E* **68**, 036125 (2003).
- [22] A. M. Ferrenberg, J. Xu, and D. P. Landau, Pushing the limits of Monte Carlo simulations for the three-dimensional Ising model, *Phys. Rev. E* **97**, 043301 (2018).
- [23] P. Hou, S. Fang, J. Wang, H. Hu, and Y. Deng, Geometric properties of the Fortuin-Kasteleyn representation of the Ising model, *Phys. Rev. E* **99**, 042150 (2019).
- [24] F. Kos, D. Poland, D. Simmons-Duffin, and A. Vichi, Precision islands in the Ising and O(N) models, *J. High Energy Phys.* **08** (2016) 036.
- [25] U. Wolff, Collective Monte Carlo Updating for Spin Systems, *Phys. Rev. Lett.* **62**, 361 (1989).
- [26] W. Wang, J. Machta, and H. G. Katzgraber, Evidence against a mean-field description of short-range spin glasses revealed through thermal boundary conditions, *Phys. Rev. B* **90**, 184412 (2014).
- [27] MPI, <https://www.open-mpi.org>.
- [28] OPENMP, <https://www.openmp.org>.
- [29] M. I. Marqués and J. A. Gonzalo, Irrelevance of canonical or grand canonical constraints near a random fixed point in large L systems, *Phys. Rev. E* **65**, 057104 (2002).
- [30] P. E. Theodorakis and N. G. Fytas, Wang-Landau study of the 3D Ising model with bond disorder, *Eur. Phys. J. B* **81**, 245 (2011).
- [31] W. Wang, R. Díaz-Méndez, M. Wallin, J. Lidmar, and E. Babaev, Melting of a two-dimensional monodisperse cluster crystal to a cluster liquid, *Phys. Rev. E* **99**, 042140 (2019).